JOURNAL OF Materials CHEMISTRY

Clean preparation of nanoparticulate metals in porous supports: a supercritical route†

Kelly S. Morley,[a] Patricia C. Marr,[a] Paul B. Webb,[a] Andrew R. Berry,[a] Francis J. Allison,[a] Grigore Moldovan,[b] Paul D. Brown[b] and Steven M. Howdle*[a]

[a]*School of Chemistry, University Park, Nottingham, UK NG7 2RD*
[b] *School of Mechanical, Materials Manufacturing Engineering and Management, The University of Nottingham, University Park, Nottingham, UK NG7 2RD*

Received 5th December 2002, Accepted 20th March 2002
First published as an Advance Article on the web 25th April 2002

Here we present the synthesis of nanometre sized silver particles which have been trapped within porous substrates; poly(styrene-divinylbenzene) beads and silica aerogels. This is the first time that supercritical carbon dioxide has been used to impregnate such porous materials with silver coordination complexes. In this paper we demonstrate that control over the resultant nanoparticles with respect to size, loading and distribution in the support material has been achieved by simple choice of the precursor complex. The solubility of the precursor complexes in the supercritical solvent is shown to be one of the key parameters in determining the size of the nanoparticles, their distribution and their homogeneity within the support matrix. Moreover, we demonstrate that the same methodology can be applied to two very different substrate materials. In the particular case of aerogels, conventional organic solvents could not be used to prepare nanoparticles because the surface tension of the solvent would lead to fracturing of the aerogel structure.

Controlled decomposition of the coordination complexes *in situ* leads to metallic silver nanoparticles with a narrow size distribution, typically 10–100 nm that are homogeneously dispersed throughout the porous substrate. The whole process is carried out at near ambient temperature and no solvent residues are introduced into the porous media. The silver precursors are specifically designed to be both CO_2 soluble and sufficiently labile to ensure facile decomposition to the metal. In-depth characterisation by X-ray diffraction and transmission electron microscopy has been applied to illustrate the homogeneous dispersion of particles throughout the composite material, determine the range and variation in particle size within the solid matrices and fully identify the resultant particles as metallic silver. This enables visualisation of dispersion and concentration, and control over particle size of the fabricated nanocomposite materials.

Introduction

Nanoscale composite materials have attracted a great deal of interest, particularly organic–inorganic hybrid nanostructures that have unique surface to volume atom ratios and associated quantum size effects.[1–4] Nanoparticulate metals of a controllable and uniform size held within a porous matrix are interesting materials for a wide range of chemical and physical applications; from catalysis to microelectronics,[5] as novel magnetic materials[6,7] and for specialised optical applications.[8] The unique properties associated with this type of material are directly related to the specific concentration, size and distribution of the particles within their host environment.[5,8–10]

Despite the wide applications of such materials, the control over particle dimensions remains the major problem associated with their fabrication by conventional techniques.[5,8] In particular, the tendency of the nanoparticles to aggregate, and the difficulty of controlling their morphology and individual particle sizes are well documented.[5,8] To prevent agglomeration, nanoparticles have previously been covered with a protective layer (mono or multi layer films[11,12]) or have been attached to a variety of support materials (microemulsion,[13] sol–gel[14,15]or polymer[6,7,16]). Use of a solid support as a medium for nanoparticle formation has been shown to stabilise the particles and to control growth on both the surface of the support and when incorporated into the internal structure.[5,8]

Conventional synthesis requires the metallic precursor to be incorporated into the porous matrix at the time of synthesis of the support. Thus, the traditional sol–gel route can be used to incorporate metal nanoparticles into the structure of aerogels.[14,15] However, high temperature is required, nanoparticles are not always achieved and agglomeration is common. Sol–gel technology cannot be applied to polymeric substrates easily. We report a technique that is able to modify the aerogel once prepared and deposit metal nanoparticles homogeneously throughout the matrix.

In contrast, the use of polymers as supports has been relatively successful.[17,18] A variety of techniques have been applied including simple mixing[19] and controlled impregnation.[20–22] The latter method has been used, for example, to prepare CdS particles dispersed in a polymer membrane leading to a material with photonic properties[23] and was fabricated by infusion of $Cd(NO_3)_2$ from an aqueous solution followed by exposure of the membrane to H_2S to yield the desired metal sulfide. The preparation of metal nanoclusters within copolymers has also been achieved by the incorporation of organometallic complexes in polymerisation by ring opening metathesis.[24–26] The metallic centres are covalently attached to each repeat unit and the complexes are then reduced to the base metal under an atmosphere of dihydrogen or by UV irradiation. However, control over particle size, homogeneity and substrate morphology is again difficult to obtain consistently. More recently dendrimers, themselves tethered to a polymeric support, have been used as templates for the formation of polymeric composites containing inorganic nanoclusters.[27,28] However, all of these techniques require the use of

†Electronic supplementary information (ESI) available: synthesis of precursor complexes; preparation of aerogels. See http://www.rsc.org/suppdata/jm/b1/b111111f/.

 DOI: 10.1039/b111111f

a considerable amount of organic solvent or involve high temperature steps that may lead to particle agglomeration and broadening of particle size distribution.

There is currently a great deal of interest on the use of $scCO_2$ to prepare free, non-supported nanoparticles. The majority of techniques formerly reported in the literature have concentrated on the production of free nanoparticles using Rapid Expansion Supercritical Solution techniques (RESS).[29–33] Here we present a method of modifying a pre-formed substrate material and have fully investigated the effects of the substrate, the precursor complex and any interaction between these and the supercritical solvent upon the resultant nanoparticles formed. In this paper we demonstrate an alternative approach to the fabrication of a wide range of porous nanocomposite materials, from polymers to aerogels, using supercritical carbon dioxide ($scCO_2$) as the processing solvent.

$ScCO_2$, (T_c = 31.1 °C, P_c = 1070.4 psi or 73.8 bar) possesses a unique combination of gas-like and liquid-like properties. Like gases, the fluid has a high diffusivity and low viscosity, but like liquids, it has appreciable densities and can dissolve coordination and organometallic species. Supercritical fluids also have zero surface tension facilitating rapid permeation and diffusion. Moreover, the density and hence solvating power of a supercritical fluid is tuneable, enabling a degree of control which is not possible using conventional solvents.[34–38] Furthermore, $scCO_2$ leaves no solvent residues (it readily dissipates as a gas upon decompression), it is recyclable and is considered to be an environmentally acceptable solvent.

The unique transport properties of supercritical fluids have been previously exploited to impregnate polymers with metal complexes and other $scCO_2$ soluble species.[21,22,39–42] Thin films of metal or metal oxide have been deposited onto a wide range of surfaces by either laser or thermally induced decomposition[43] or more recently onto microelectronic devices and other surfaces.[36,44–47] Both spectroscopic and theoretical modelling investigations have also been carried out to investigate the specific interactions between the support matrix and the carrier solvent involved in the supercritical impregnation process.[22,40,48–50] Indeed, Watkins *et al.*[51] also made the first report of the preparation of composite materials using $scCO_2$ assisted infusion of $PtMe_2$(COD) into poly(4-methylpent-1-ene) and poly(tetrafluoroethylene), leading to the formation of Pt nanoparticles. Wide-angle X-ray diffraction confirmed the presence of metallic platinum and TEM was used to observe the distribution in the support. For the first time we report a statistical analysis of the particle size distributions and link the particulate formation, homogeneity within the support and dimensions of the particles to the solubility of the precursor within the supercritical solvent.

Our focus in this paper is the development of specifically designed silver precursor complexes leading to controlled metallic nanoparticles. The route involves infusion of the metal complex into two very different solid matrices; poly(styrene-divinylbenzene) beads and silica aerogels. The precursor metal complex is then reduced to silver metal nanoparticles using hydrogen, followed by a simple $scCO_2$ extraction step undertaken to remove ligand residues from the composite material. We investigate the relationship between the metal precursor complex used in the impregnation process and the structure and size distributions of the resultant nanoparticles. Detailed characterisation (both TEM and XRD) of the nanocomposite materials will be described. A second research objective is to optimise the ligand structure to achieve high precursor volatility and efficient impregnation. The precursor complexes must be soluble in $scCO_2$ **and** undergo facile decomposition to the desired metal releasing the organic ligand residues.

There has been extensive research into the development of both CO_2 soluble metal complexes for catalysis and CO_2 soluble chelating ligands for chelation–extraction of heavy metals from contaminated water streams.[52] The properties required of the precursor complexes for the impregnation technique described are also inherent in metal β-diketonates, a class of complexes often used in chemical vapour deposition processes.[53,54] We have focused upon silver precursors of the general form Ag(hfpd)L where hfpd = 1,1,1,5,5,5-hexafluoropentane-2,4-dione and L = 1,1,4,7,10,10-hexamethyltriethylene for complex [A], L = tetraethylene glycol dimethyl ether for complex [B] (See Table 1). The most effective CO_2-philes known are fluorocarbons[55] and this has been exploited in the design of the precursor complexes used in this process. The use of such encapsulating ligands in the design of the complex decreases their volatility, but enhances the solubility properties of the precursor complex by shielding the metal centre so that the $scCO_2$ encounters only a hydrophobic shell. In this paper we highlight the modification of a pre-formed support matrix to produce a homogeneous dispersion of metal particles trapped within the substrate.

Experimental

All syntheses were carried out under an inert atmosphere using standard Schlenk techniques and cannula transfer. All solvents were dried and degassed prior to use and stored over 4 Å molecular sieves. All reagents were obtained from Aldrich Chemical Co. and were used without further purification. 1,1,1,5,5,5-Hexafluoropentane-2,4-dione (H-hfpd) was stored under an inert atmosphere. Products were treated as air/moisture and light sensitive and stored in dark bottles under an inert argon atmosphere. Elemental analyses were obtained from the microanalytical service at The University of Nottingham School of Chemistry. Mass spectra were obtained using a Vacuum Generators VG 70E micromass spectrometer. ^1H, ^{13}C and ^{19}F NMR spectra were obtained on a Bruker DPX300 spectrometer. Infrared spectra were recorded on Nicolet Avatar 360 FTIR spectrometer.

The synthesis of silica aerogels and the precursor coordination complexes of sliver followed standard literature procedures[56–58] and details are summarized in the ESI.†

Poly(styrene-DVB) resin beads were used as supplied.[59] The poly(styrene-DVB) resins contain residues of monomer and conventional solvent from the standard synthetic procedures employed in their synthesis. These residues were removed during the impregnation process (*vide infra*). However, in order to allow quantification of the mass uptake of silver, we first treated all poly(styrene-DVB) resins with a $scCO_2$ extraction step to remove all volatiles remaining from the resin synthesis; typically a level of *ca.* 3.7 wt%. All of the poly(styrene-DVB) resins reported in this paper were pre-treated in this way with $scCO_2$ by placing the sample (*ca.* 0.2 g) in a stainless steel autoclave (10 ml volume; Thar Designs) and purged with $scCO_2$ for 24 h at *ca.* 1500 psi and 35 °C.

Nanoparticle synthesis

The complex Ag(hfpd)L (0.17 g) and either silica aerogel (0.4 g) or poly(styrene-DVB) beads (0.21 g) were placed in a 10 ml

Table 1 Coordination precursor complexes used in the impregnation process

Ag(hfpd) tetraamine [A]	Ag(hfpd) tetraglyme [B]
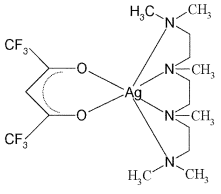	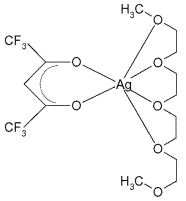

stainless steel autoclave (Thar Designs). The autoclave was filled with CO_2, and the pressure and temperature increased to 4000 psi and 40 °C respectively. These conditions were chosen because they provided the optimum loading of metal complex into the porous substrate.[60] After 24 h under these conditions the CO_2 was released over a period of *ca.* 5 min. The autoclave was then filled with hydrogen to a pressure of 1000 psi and the temperature increased to 60 °C. This allowed for full decomposition of the metal coordination complex. After 48 h the H_2 was released from the cell over a period of *ca.* 5 min and the autoclave was purged with CO_2 for a further 24 h at 4000 psi and 40 °C. The long time intervals were chosen to ensure complete conversion. The pressure was then released over a period of *ca.* 5 min and the sample removed from the autoclave. These conditions were used for the preparation of all of the nanocomposites described in this work.

Analysis of composites

Determination of the uptake of metal into the solid support was achieved through measurement of the mass of the substrate before and after the impregnation process. Powder X-ray data were acquired using a Philips EXPERT system fitted with a PW1710 diffractometer control unit with Cu-Kα radiation, (λ = 1.5405 Å). The samples were ground up before loading onto an indented glass plate and representative diffractograms were acquired over 20–80° (2θ) with 0.02° steps and 4 s acquisition times per step. The PC IDENTIFY program was used to assess the purity of the samples by comparison to the JCPDS database. APD Philips software was used for indexing and phase determination. Crystallite sizes were estimated using the APD program and by applying the Scherrer equation to the XRD line-widths of the different reflections.[61] Transmission Electron Micrograph (TEM) images were collected using a JEOL JEM-2000FX II electron microscope operating at 200 keV. The samples were ground up in preparation for TEM analysis and a suspension of the solid matrices were sonicated in methanol for a short time before 2–3 drops of the suspension were transferred onto a 3 mm diameter holey carbon coated copper grid. The solvent was allowed to evaporate at room temperature before loading the sample in the microscope. Conventional bright field imaging was used to observe the particle morphology, while diffraction patterns confirmed the atomic plane spacings to be consistent with that of elemental silver.

Statistical analysis of particle size was achieved by means of a digitised mapping procedure. TEM micrographs were initially transformed into binary images and the projected areas of the individual particles were determined using Scion Image. Particle size distribution data were then calculated for all of the samples using the descriptive statistics function in Excel. Three TEM micrographs acquired from different regions were analysed for each sample and the values averaged.

Synthesis of precursor complexes

[1]Ag(hfpd)$_2$(OH$_2$)$_2$. To a slurry of silver(I) oxide (2.78 g, 12.0 mmol) in THF (*ca.* 40 ml), H-hfpd (3.4 ml, 24.0 mmol) was added dropwise with vigorous stirring and left for 1 hour until the dissolution of Ag_2O was complete. The solution was filtered and the solvent removed *in vacuo* to yield a white precipitate. The crude product was purified by dissolution into minimum amount of hot THF and allowed to crystallise at 4 °C, yielding colourless square crystals (6.245 g, 80.3%, mp 146–148 °C).

Analysis calculated for ($C_{10}H_6AgF_{12}O_6$): expected (Found) C 21.53% (23.64%), H 1.15% (1.21%). ^{1}H NMR (300.13 MHz, DMSO, 300 K): δ = 5.35 (s, 2H, C*H*), 3.70 (s, 2H, O*H*$_2$) ppm. ^{19}F NMR (282.4 MHz, DMSO, 300 K): δ = −71.14 (CF_3). IR (Nujol Mull)(ν/cm^{-1}) (s = strong, m = medium, w = weak): 2914.5 s, 1663.0 s, 1631.3 s, 1603.2 s, 1558.4 s, 1501.7 s, 1460.1 s, 1376.9 m, 1326.3 m, 1264.4 s. FAB Positive ion mass spectrum (NBA): *m*/*z* 563 {[Ag(hfac)$_2$(OH$_2$)$_2$]$^+$, 12.7%}, 538 {[Ag(hfac)$_2$OH$_2$]$^+$, 24.6}, 519 {[Ag(hfac)$_2$]$^+$, 11.2}, 413 {[Ag(OC(CF$_2$)CHC(CF$_2$)O)$_2$]$^+$, 62}, 347 {[Ag(OH$_2$)$_2$(hfac)]$^+$, 100}, 260 {[Ag(OC(CF$_2$H)CHC(CFH$_2$)O]$^+$, 58.79}, 136 {HFCCOCH$_2$COCFH]$^+$, 30.1}, 108 {[Ag]$^+$, 95%}.

[A] Ag(hfpd)(tetraamine). To a solution of the homoleptic **[1]**, (6.245 g, 12.0 mmol), in THF (*ca.* 40 ml), at 0 °C 1,1,4,7,10,10-hexamethyltriethylene tetraamine (2.76 g, 12.0 mmol), was added dropwise. The solution was stirred vigorously for 1 hour until the dissolution of Ag_2O was complete. The solution was filtered and the solvent removed *in vacuo* to yield a yellow precipitate. The crude product was recrystallised from a THF solution, layered with pentane at −20 °C to yield yellow needle-like crystals (10.37 g, 83.9%, 76–78 °C).

Analysis calculated for ($C_{17}H_{31}AgF_6N_4O_2$): Expected (Found) C 37.51% (37.39%), H 5.56% (5.67%), N 10.29% (10.21%).

^{1}H NMR (300.13 MHz, DMSO, 300 K): δ = 5.24 (s, 1H, C*H*), 2.50 (m, 12H, (CH$_3$)$_2$(NC*H*$_2$)$_2$(CH$_3$)(C*H*$_2$)$_2$N(CH$_3$)(C*H*$_2$)$_2$N(CH$_3$)$_2$), 2.47 (s, 12H, (C*H*$_3$)$_2$(NCH$_2$)$_2$(CH$_3$)(CH$_2$)$_2$N(CH$_3$)(CH$_2$)$_2$N(C*H*$_3$)$_2$), 2.35 (s, 6H, (CH$_3$)$_2$(NCH$_2$)$_2$(C*H*$_3$)(CH$_2$)$_2$N(C*H*$_3$)(CH$_2$)$_2$N(CH$_3$)$_2$), ppm. ^{13}C NMR (75.15 MHz, DMSO, 300 K): δ = 173.6 (q, CO), 118.3 (q, CF_3), 84.3 (s, CH), 58.9 (s, CH_2), 55.7 (s, CH_2), 48.3 (s, N(CH$_3$)$_2$), 43.9 (s, NCH$_3$) ppm. ^{19}F NMR (282.4 MHz, DMSO, 300 K): δ = −76.11 (CF_3). IR (Nujol Mull)(ν/cm^{-1})(s = strong, m = medium, w = weak): 2922.7 s, 2853.0 s, 1664.0 s, 1543.4 s, 1526.9 s, 1461.9 s, 1377.0 m, 1313.3 m, 1244.4 s. FAB Positive ion mass spectrum (NBA): *m*/*z* 340{[Ag(CH$_3$)$_2$NCH$_2$CH$_2$N-(CH$_3$)CH$_2$CH$_2$N(CH$_3$)CH$_2$CH$_2$N(CH$_3$)$_2$]$^{2+}$, 13%}, 339{[Ag-(CH$_3$)$_2$NCH$_2$CH$_2$N(CH$_3$)CH$_2$CH$_2$N(CH$_3$)CH$_2$CH$_2$N(CH$_3$)$_2$)]$^+$, 92}, 338{[Ag(CH$_3$)$_2$NCH$_2$CH$_2$N(CH$_3$)CH$_2$CH$_2$N(CH$_3$)-CH$_2$CH$_2$N(CH$_2$)(CH$_3$)]$^+$,16}, 337{[Ag(CH$_3$)$_2$NCH$_2$-CH$_2$N(CH$_3$)CH$_2$CH$_2$N(CH$_3$)CH$_2$CH$_2$N(CH$_2$)$_2$]$^+$, 100}, 229{[(CH$_3$)$_2$NCH$_2$CH$_2$N(CH$_3$)CH$_2$CH$_2$N(CH$_3$)CH$_2$CH$_2$N-(CH$_3$)$_2$]$^+$, 7}, 115 {[(CH$_3$)$_2$NCH$_2$CH$_2$NCH$_3$)$_2$]$^+$, 5}, 72{[(CH$_3$)$_2$-NCH$_2$CH$_3$)]$^+$, 23}, 58{[N(CH$_3$)$_3$]$^+$, 14%}.

[B] Ag(hfpd)(tetraglyme). To a slurry of silver(I) oxide, (2.78 g, 12.0 mmol) and tetraethylene glycol dimethyl ether (5.33 g, 24.0 mmol) in THF (*ca.* 40 ml), H-hfpd (3.40 ml,24.0 mmol) was added dropwise with vigorous stirring and left for 1 hour until the dissolution of Ag_2O was complete. The solution was filtered and the solvent removed *in vacuo* to yield an off white precipitate. The crude product was recrystallised from a THF solution layered with pentane (*ca.* 20 ml), at −20 °C to yield colourless square-shaped crystals (8.76 g, 67.4%, mp 46–48 °C).

Analysis calculated for ($C_{15}H_{23}AgF_6O_6$): Expected (Found) C 33.54% (33.50%), H 4.32% (4.10%). ^{1}H NMR (300.13 MHz, DMSO, 300 K): δ = 5.29 (s, C*H*), 3.53 (m, 8H, CH$_3$OC*H*$_2$-C*H*$_2$OCH$_2$CH$_2$O-), 3.48 (m, 4H, CH$_3$OCH$_2$CH$_2$OC*H*$_2$CH$_2$O-), 3.42 (m, 4H, CH$_3$OCH$_2$CH$_2$OCH$_2$C*H*$_2$O-), 3.24 (s, 6H, C*H*$_3$) ppm. ^{13}C NMR (71.15 MHz, DMSO, 298 K): δ = 83.3 (CH$_3$), 71.8 (CH$_2$), 70.3 (CH$_2$), 70.1 (CH$_2$), 58.6 (CH$_3$) ppm. ^{19}F NMR (282.40 MHz, DMSO, 300 K): δ = −76.11 (C*F*$_3$) ppm. IR (Nujol Mull)(ν/cm^{-1})(s = strong, m = medium, w = weak): 2857.4 s, 1663.2 m, 1524.9 m, 1463.6 m, 1376.7 m, 1357.3 m, 1253.2 m, 1191.3 w, 1169.5 w, 1169.48 w, 1149.5 w, 1095.3 w, 1026.7 m, 942.4 m. FAB Positive ion mass spectrum (NBA): *m*/*z* 331{[Ag(CH$_3$OCH$_2$CH$_2$OCH$_2$CH$_2$OCH$_2$CH$_2$OCH$_2$-CH$_2$OCH$_3$)]$^+$, 91%}, 329 {[Ag(CH$_2$OCH$_2$CH$_2$OCH$_2$CH$_2$OCH$_2$-CH$_2$OCH$_2$CH$_2$OCH$_2$)]$^+$, 100}, 245{[Ag(hfpd)]$^+$ − CF$_3$, 55}, 109 {[Ag]$^+$, 15}, 107 {[CF$_2$COCH$_2$CH$_3$)]$^+$, 17}, 59 {[HOCH$_2$-CH$_2$CH$_3$]$^+$, 17%}.

Preparation of aerogels. A solution of hydrochloric acid (1 M, 6 drops) in ethanol (7.7 g, 0.17 mol) and water (5.6 g, 0.31 mol) was added dropwise to a mixture of *N*,*N*-dimethylacetamide (10.88 g, 0.13 mol) and tetraethoxysilane

Table 2 Change in mass of support matrix post-impregnation

	Aerogel matrix		Poly(styrene-DVB) matrix	
Complex	[A]	[B]	[A]	[B]
Mass/g of Ag	0.0441	0.0322	0.0344	0.0363
Mass/g of matrix pre-impregnation	0.5727	0.3795	0.1997	0.1860
Mass/g of matrix post-impregnation	0.5838	0.4129	0.2059	0.2049
Mass increase/g	0.0111	0.03154	0.0062	0.0189
Increase in wt (%)	1.94	8.80	3.10	10.16

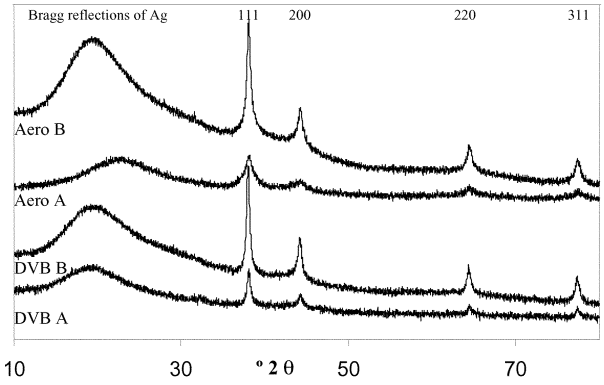

Fig. 1 XRD trace of impregnated substrates

(5.20 g, 0.25 mol). The mixture was stirred for 1 hour at room temperature (TEOS–EtOH–H_2O–DMA = 1 : 0.7 : 1.25 : 0.5). A solution of ammonium hydroxide (6 drops) in ethanol (7.7 g, 0.17 mol) and water (5.6 g, 0.31 mol) was added, and the mixture stirred for a further 20 min at room temperature. The gels were aged and dried under identical conditions. After synthesis as described, the samples were held in an oven at 30 °C for 18 h before being stored at room temperature for seven days. After this time, the alcogels were removed from their beakers, broken into cubes of width *ca.* 2 cm and stored under methanol. The aerogel synthesis was completed by an $scCO_2$-drying step. The alcogel sample was placed in a stainless steel autoclave (10 ml, Thar Designs), and the autoclave filled with methanol. The cell was purged with CO_2 for 2 h at 1500 psi and 20 °C and for a further 20 h at 1500 psi and 30 °C. The pressure in the cell was then released over a period of *ca.* 30 min until atmospheric pressure was reached. The sample was removed from the autoclave and placed in an oven at 30 °C for 48 h.

Results

There were noticeable changes in the colouration of the materials after processing. The aerogels were opaque prior to processing, but after impregnation showed a marbled exterior with a very clear pale yellow colour throughout the bulk. This indicates the presence of colloidal silver that has an absorption band at 410 nm.[62] The polymer beads were initially white but after impregnation and reduction were uniformly brown in colour. In all cases, at the intermediate stage (after impregnation, but before reduction of the complexes with hydrogen) the matrices took on the colour of the silver complexes.

Coordination precursors [A] and [B] (see Table 1) yielded nanoparticles of silver metal in both the silica aerogels and poly(styrene-DVB) beads after processing with $scCO_2$. Substantial changes in the mass of the samples indicated the presence of silver and the loading of the metal in the support has been quantified (see Table 2). A broad range of alkane and thioether based Ag(hfpd) species have also been synthesised, but were found to be unstable or to have very low solubility in CO_2; the thioether complexes readily form polymeric species and these are reported elsewhere.[63,64]

The powder X-ray diffraction patterns obtained for all of the samples yielded reflections that could be attributed to elemental silver (See Fig. 1). No other elemental or compound reflections were observed in the diffractograms signifying complete reduction and removal of the precursor complex. X-Ray diffraction measurements of the aerogel and poly(styrene-DVB) composite materials gave four Bragg reflections (see Table 3) that were indexed to the (111), (200), (220) and (311) reflections of metallic silver by reference to the JCPDS file 04-0783. In the case of both the aerogel and poly(DVB-styrene) samples, a broad band was also present in all XRD patterns which is attributed to the amorphous bulk substrate material. The relative intensity of the reflections in the diffractograms also indicates the concentration of silver particles in the two matrices. From the diffractograms collected (see Fig. 1) it is clear that more intense reflections are observed and therefore higher concentrations of silver present in the support, when complex B is utilised as the precursor complex. XRD has therefore confirmed the presence of free metallic silver within both the aerogel and the poly(styrene-DVB) samples. The particle/crystallite sizes have been estimated from the full-width at half maxima of the XRD reflection using Scherrer's formula (see Table 4).

Table 4 Crystallite sizes determined from XRD analysis

Substrate	Complex	Crystallite size/nm
Aerogel	[A]	7
	[B]	18
Poly(DVB-styrene)	[A]	23
	[B]	25

Bright field TEM micrographs have been obtained for all of the impregnated samples and illustrate the fine dispersion of the particles within the matrix (see Figs. 2–5). Diffraction ring patterns have also been obtained corresponding to the nanoparticles observed and the interplanar spacings of these are consistent with the XRD data collected and the JCPDS file 04-0783 for metallic silver (see Table 5). Digitised analysis has been carried out on the TEM micrographs using a particle mapping technique to yield statistically significant particle size distribution data for each sample (see Figs. 6–9 and Table 6).

Discussion

Analysis of both types of porous substrate using TEM and powder XRD provides clear evidence of formation of metallic nanoparticles. In addition, substantial increases in mass were

Table 3 XRD peak positions

Support matrix	Precursor complex	*d* spacing and corresponding lattice plane			
Reference	JCPDS 04-783	[111] 2.3618	[200] 2.0470	[220] 1.4452	[311] 1.2310
Aerogel matrix	[A]	2.3605	2.0495	1.4436	1.2312
	[B]	2.3670	2.0495	1.4460	1.2332
Poly(DVB-styrene) matrix	[A]	2.3620	2.0457	1.4444	1.2324
	[B]	2.3663	2.0495	1.4463	1.2330

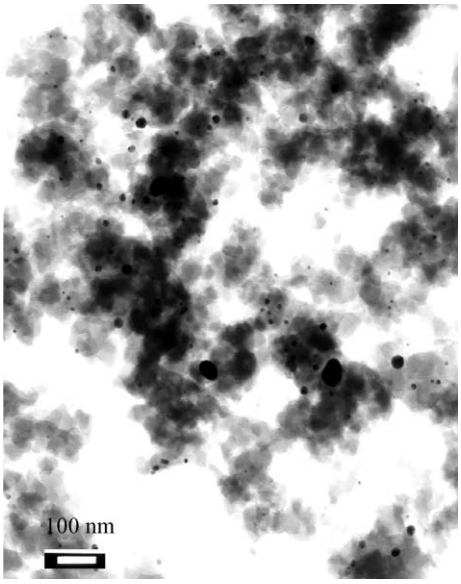

Fig. 2 TEM image of poly(styrene-DVB) matrix impregnated with complex [A].

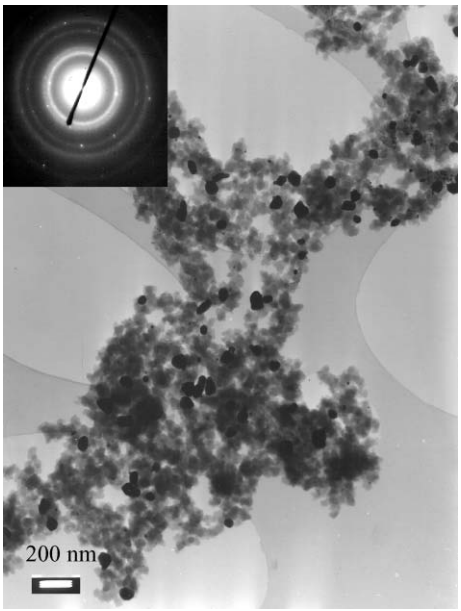

Fig. 3 TEM image of poly(styrene-DVB) matrix impregnated with complex [B] and corresponding ring diffraction pattern.

observed ranging between 1.9–10.2% by weight. The uptake for the polymeric substrate was found to be consistently higher than the aerogel (see Table 2). The higher loading obtained for poly(styrene-DVB) is almost certainly a result of the high surface area of the support exposed during impregnation. Poly(styrene-DVB) used throughout this study was in the form of small beads, in contrast to the 2 cm^3 block of aerogel. This is likely to facilitate more effective impregnation by increased partitioning of the precursor complex from $scCO_2$ into the solid matrix. However, a much more striking difference was noted

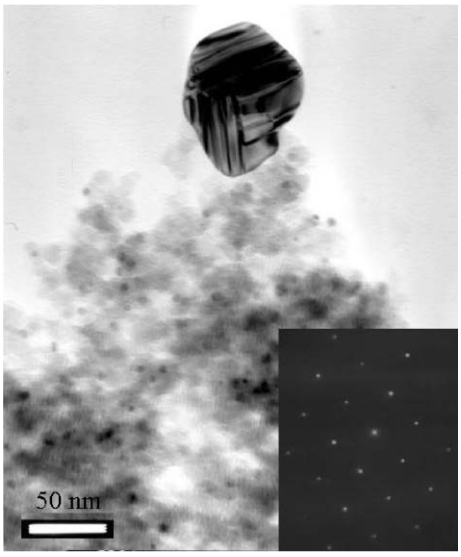

Fig. 4 TEM image of silica aerogel matrix impregnated with complex [A] and corresponding diffraction pattern (111 plane of metallic silver).

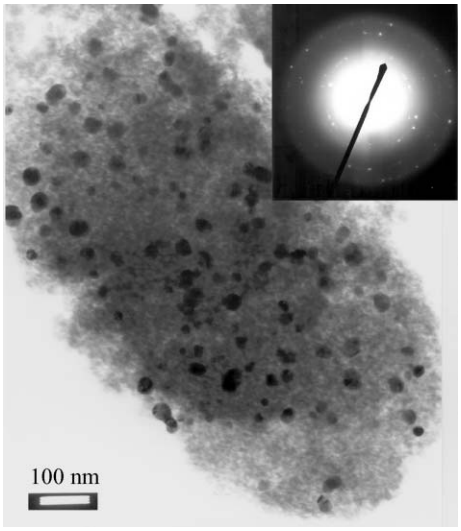

Fig. 5 TEM image of silica aerogel matrix impregnated with complex [B] and corresponding ring diffraction pattern.

between the two precursor complexes. A lower loading of metallic silver was observed in both supports when using complex [A] (1.9% by wt in the aerogel matrix and 3.1% by wt in poly(styrene-DVB)) compared to [B] (8.8% by wt in the aerogel matrix and 10.2% by wt in poly(styrene-DVB)) (see Table 2). This is also supported by the appearance of more intense reflections in the X-ray diffractograms when complex B is utilised as the precursor complex for the impregnation of both matrices.

Particle analysis

XRD and TEM analysis have confirmed the presence of metallic silver nanoparticles in the porous substrates. The four characteristic reflections of the powder XRD diffractogram

Table 5 *d* spacings determined from TEM analysis

Support matrix	Precursor complex	*d* spacing			
Reference	JCPDS 04-783	[111] 2.3590	[200] 2.0440	[220] 1.4450	[311] 1.2310
Aerogel matrix	[A]	2.36	2.05	1.43	1.21
	[B]	2.38	2.05	1.42	1.22
Poly(DVB-styrene) Matrix	[A]	2.38	2.04	1.46	1.25
	[B]	2.34	2.04	1.46	1.24

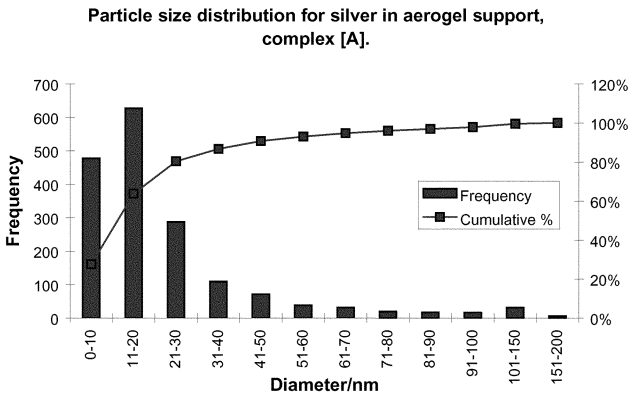

Fig. 6 Particle size distribution data for complex [A] dispersed in silica aerogel.

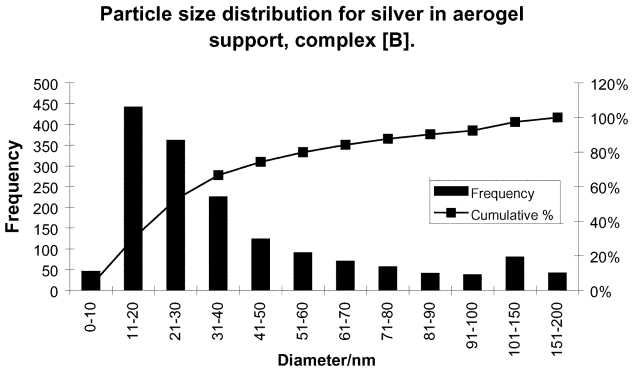

Fig. 7 Particle size distribution data for complex [B] dispersed in silica aerogel.

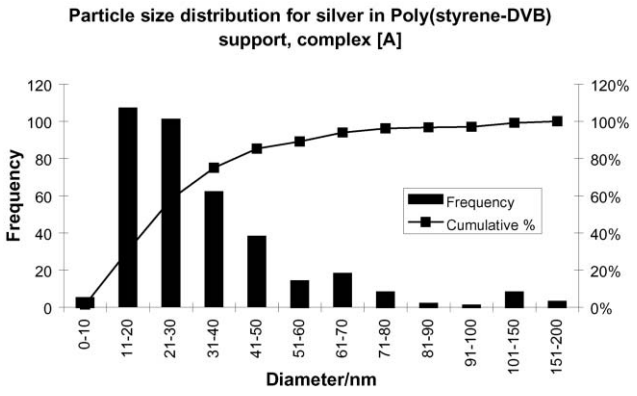

Fig. 8 Particle size distribution data for complex [A] dispersed in poly(styrene-DVB).

Table 6 Particle sizes determined from TEM data and particle mapping

		Particle diameter/nm and statistical values			
Support matrix	Precursor complex	Mean	Standard deviation	Mode	Standard error
Aerogel Matrix	[A]	23.2	22.7	9.6	0.55
	[B]	41.6	35.2	15.8	0.88
Poly(DVB-styrene) matrix	[A]	33.7	24.6	18.4	1.29
	[B]	42.3	32.0	22.5	0.96

agree closely with those obtained from TEM by selected area diffraction patterns and are consistent with the known silver interplanar spacings. No other peaks or rings were observed for silver containing species in either XRD or TEM respectively. The average particle sizes have been determined by both XRD and particle mapping of the TEM images. Below we compare the experimental data obtained on each sample (see Tables 4 and 6, Figs. 6–9).

Powder XRD data on the composites prepared from complex [A] show silver nanoparticles in the aerogel matrix having the smallest average domain size (7 nm) seen in this study. This is consistent with the size of particles observed in the TEM images and the mode particle size value (9.6 nm) calculated by particle mapping. Particles resulting from impregnation of complex [B] in the silica aerogel matrix were much larger (18 nm by XRD, 15.8 nm by TEM). Impregnation of the poly(styrene-DVB) matrix with complex [A] produced nanoparticles of silver which were larger than those seen in the aerogel matrix (23 nm by XRD, 18.4 nm by TEM), while complex [B] led to the largest average size of nanoclusters (25 nm by XRD, 22.5 nm by TEM) dispersed throughout the polymer matrix. The particle dimensions determined from both XRD and TEM data are consistent within the limitations of the experimental and analytical techniques employed, *i.e.* ± 5 nm for XRD, ± 1 nm for TEM (see Tables 4 and 6).

There is a clear discrepancy between the data values calculated for the average particle dimensions. Larger average particle sizes are consistently determined by XRD when compared to those values calculated by statistical analysis of the TEM micrographs. This may be explained by the presence of larger platelets of silver observed on the surface of some of the samples. The process of supercritical impregnation of the support matrices necessarily results in some surface coating and these larger micron sized metallic flakes were observed on the surface of both matrices. Indeed, this coating technique has been optimised to form the basis of supercritical fluid coating deposition processes.[44,45] Since XRD is performed on the whole sample, sampling a larger volume than TEM, then

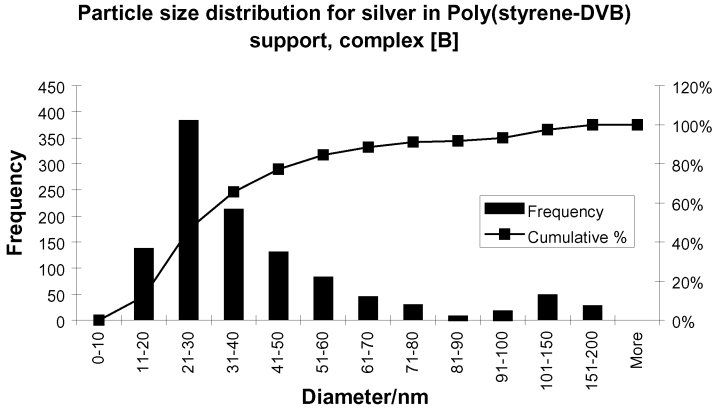

Fig. 9 Particle size distribution data for complex [B] dispersed in poly(styrene-DVB).

the flakes will contribute to the XRD powder line widths observed and measured for these samples. However, TEM is a narrow sampling technique and the particle mapping procedure employed for TEM allows one to overlook the larger surface flakes and eliminate them from the statistical data of the TEM images. The difference in the particle size determined by XRD and TEM reflects this line of reasoning. However, the key observation is that the differences observed are small; clearly demonstrating that the contribution of surface deposition is minor and the silver is substantially in the form of discrete nanoparticles. Our data clearly illustrate the necessity of combining complementary techniques for such analyses.

TEM analysis

Larger clusters of silver (*ca.* 50 nm) were more frequently observed in the poly(styrene-DVB) matrix and reflect the influence of that particular matrix leading to a higher degree of aggregation of particles and a wider distribution of particles size (see Figs. 2 and 3). For the aerogel samples, TEM clearly demonstrates a very fine dispersion of silver particles in the aerogel. Fewer large clusters were observed in the aerogel in comparison to the poly(styrene-DVB) support. Since the accumulation of atoms to form particles visible on the TEM scale is essentially diffusion limited, the process is highly dependent upon the concentration of atoms held in the solid matrix. Thus, the consistently higher loading for each complex in the poly(styrene-DVB) support may well be the significant factor in influencing the formation of a higher population of the larger clusters.

Analysis of the materials by TEM has also allowed particle texture, size and crystallographic structure to be studied and enabled a mechanism of particle growth to be postulated. TEM has revealed elongation and a degree of faceting around the edges of the majority of particles. Fig. 4 clearly illustrates the planar defects, *i.e.* internal twinning, and faceting, of a large (50 nm) particle that suggests particle evolution proceeds by a twin mediated growth process. These deformations are not stress induced and the mechanism of growth is therefore limited by diffusion during the decomposition of the precursors when enough energy must be available for the individual atoms of silver to move and aggregate to form the particles visible on the TEM scale. There must be catchment areas for particulate growth and the only limitation to growth is therefore diffusion of the atoms through the matrix to the nucleation site. The suggestion is that decomposition of the precursor occurs at the surface of the growing silver particles. This atom-by-atom, layer upon layer growth mechanism is apparent for all of the samples analysed.

Metal loading and solubility. The results obtained demonstrate that there are significant differences exerted by the two matrices upon nanoparticle size distribution and loading. However, the most significant differences arise from the two complexes studied.

The solubility of the two complexes in $scCO_2$ has been determined using an *in situ* FTIR technique.[60] Here, careful measurement of the solubility isotherms of each complex at 37 °C over a broad pressure range demonstrate that the complex [A] has a much lower solubility than [B] in $scCO_2$. Indeed, at 37 °C and 2500 psi there is a factor of three difference in the relative solubilities of [A] (0.025 mol l^{-1}) to [B] (0.075 mol l^{-1}).

Thus, we speculate that the lower distribution of silver particles seen in both matrices when precursor [A] is utilised results from the low solubility of this complex in the carrier solvent. The limited solubility and therefore limited transfer of complex [A] into the support matrix affords a lower loading of particles in the composite. In addition, the lower solubility also supports the clear observation that in all samples created using complex [A] the dispersion of silver particles has been shown to be inhomogeneous throughout both matrices. In addition, the mechanism for particle growth and limiting aggregation is dependent upon diffusion and hence upon the concentration of particles. Thus, one might predict that there would be a smaller particle size observed at the lower particle concentration. The presence of surface platelets is much more noticeable with the samples prepared from precursor [A] and this also is associated with the lower solubility in $scCO_2$ and hence a more favourable interaction between the complex and the matrix over that of the complex and the solvent.[60] TEM analysis of the composites produced using [A] has also illustrated areas of the support containing none or very few silver particles. This was not the case for [B] where nanoparticles were observed in all regions of the samples examined by TEM (see Figs. 2–5).

The impregnation of both matrices with complex [B] led to the much higher loadings of metallic silver particles than for complex [A]. Here, the solid matrix clearly supports a higher quantity of silver particles with a wider particle size distribution. This again relates to the solubility of the precursor complex in the carrier solvent. Since the complex is highly soluble in $scCO_2$, yet the interaction with the support is still favourable, then the complex will infuse all the way through the solid material and be homogeneously deposited throughout the support matrix. The silver complex is dispersed homogeneously throughout the support and upon reduction of the complex by hydrogen the particles of silver that are formed are essentially closer together and so diffusion of the atoms to a nucleation site is therefore facile and aggregation occurs. This results in a much wider range in particle size, whilst dispersion homogeneity throughout the whole matrix is maintained.

An additional factor is that complex [A] is also slightly less stable and degrades more readily than complex [B], which may also be an important factor in control over particle size and distribution in the support. Further work needs to be done to qualify the effects of this thermal stability upon the nanocomposite materials. The molecular diameter of the complexes might also be important. [A] is larger than [B] and others[65] have demonstrated that for the extraction of uranium by supercritical fluid extraction a smaller molecular diameter facilitated greater diffusion and enabled thorough extraction of the desired metal.

Conclusion

Composite materials have been produced through a supercritical impregnation process using $scCO_2$ as the only solvent. Exposure to air, ultra-violet light and heat have all been reported as methods for controlled decomposition of such coordination complexes to free metal and ligand residues.[66] However, when dealing with support materials any change or response to the decomposition process by the matrix must be considered. Clearly high temperature methods are not applicable to polymeric systems and the use of conventional organic solvents is not possible with the aerogel matrix described. In this work the coordination complexes are reduced by H_2, yielding clean decomposition products. The ligands are then removed from the substrate by $scCO_2$ extraction. This leaves pure metal nanoparticles behind in the support with no apparent change to the pre-formed support material.

XRD analysis of the samples has unequivocally identified the particles held in both support matrices to be metallic silver. TEM images of the samples have also substantiated these findings. TEM images have allowed us to determine size dependency of resultant particles and homogeneity with respect to the distribution within the solid support. This is believed to depend greatly on the solubility of the precursor complex in the carrier solvent and partitioning of the complex between the solvent and support. High solubility in the solvent results in a homogeneous distribution of metallic particles with a wider

range in particle size. However, low solubility in the solvent, results in an inhomogeneous dispersion of particles throughout the matrix due to partitioning of the complex between the matrix and the carrier solvent. Aggregation of particles towards the edge/surface of the composite material is also observed more frequently when the complex has limited solubility in $scCO_2$. Further work and development of this impregnation process is currently on going and we will report the effects of complex stability, size and solubility upon the process of nanocomposite synthesis.

For the first time, we have demonstrated the impregnation of aerogel and polymeric supports using silver coordination complexes and $scCO_2$ as the only solvent. Control of solubility through design of the precursor complex leads to control over the dispersion and concentration of metal particles throughout the support and the size distribution of the resulting particles. The variation in nanoparticulate formation has been discussed with reference to both the substrate material and the precursor complex involved in the synthesis. A mechanism to particle formation has also been postulated. Further studies relating to the enhancement of associated properties of the composite materials produced; isolation of the degradation products; and kinetics of degradation; are under investigation and will be reported in the near future.

Acknowledgement

We are grateful to the EPSRC (studentship support to KSM), Perplas Medical Ltd and to the University of Nottingham Institute for Materials Technology (UNIMAT). We are also grateful to Prof D.C. Sherrington[59] for kindly supplying the Poly(styrene-DVB) resin beads.

References

1 A. Heinglein, *Top. Curr. Chem.*, 1988.
2 A. Heinglein, *Chem. Rev.*, 1989, **89**, 1861.
3 G. C. Bond, *Surf. Sci.*, 1985, **156**, 966.
4 J. H. Fendler, *Nanoparticles and Nanostructured Films*, ed. J. H. Fendler, Wiley-VCH, Chichester, 1998.
5 A. Y. Stakheev and L. M. Kustov, *Applied Catal. A*, 1999, **188**, 3.
6 J. Ramos, A. Millan and F. Palacio, *Polymer*, 2000, **41**, 8461.
7 C. Castro, J. Ramos, A. Millan, J. Gonzalez-Calbet and F. Palacio, *Chem. Mater.*, 2000, **12**, 3681.
8 L. L. Beecroft and C. K. Ober, *Chem. Mater.*, 1997, **9**, 1302.
9 F. Hache, D. Ricard and C. Flytzanis, *J. Opt. Soc. Am. B*, 1986, **3**, 1647.
10 C. Voisin, D. Christofilos, N. D. Fatti, F. Vallee, B. Prevel, E. Cottancin, J. Lerme, M. Pellarin and M. Broyer, *Phys. Rev. Lett.*, 2000, **85**, 2200.
11 K. Akamatsu and S. Deki, *Nanostruct. Mater.*, 1997, **8**, 1121.
12 N. E. Fernandes, S. M. Fisher, J. C. Poshusta, D. G. Vlachos, M. Tsapatsis and J. J. Watkins, Reactive Deposition of Metal Thin Films within Porous Supports from Supercritical Fluids, *Chem. Mater.*, 2001, **13**, 2023.
13 Y. D. Yin, X. L. Xu, C. J. Xia, X. W. Ge and Z. C. Zhang, *Chem. Commun.*, 1998, 941.
14 L. Schmid, O. Krocher, R. A. Koppel and A. Baiker, *Microporous Mesoporous Mater.*, 2000, **35-6**, 181.
15 M. Kawashita, S. Tsuneyama, F. Miyaji, T. Kokubo, H. Kozuka and K. Yamamoto, *Biomaterials*, 2000, **21**, 393.
16 L. Wang, M. Rocci-Lane, P. Brazis, C. R. Kannewurf, Y. I. Kim, W. Lee, J. H. Choy and M. G. Kanatzidis, *J. Am. Chem. Soc.*, 2000, **122**, 6629.
17 D. Donescu, *Mater. Plast. (Bucharest)*, 2001, **38**, 3.
18 J. F. Ciebien, R. T. Clay, B. H. Sohn and R. E. Cohen, *New J. Chem.*, 1998, **22**, 685.
19 C. E. Carraher and R. Seymour, *Polymer Chemistry: An Introduction*, ed. J. J. Lagowski, Marcel Dekker, New York, 1996.
20 K. I. Alder and D. C. Sherrington, *Chem. Commun.*, 1998, 131.
21 P. B. Webb, P. C. Marr, A. J. Parsons, H. S. Gidda and S. M. Howdle, *Pure Appl. Chem.*, 2000, **72**, 1347.
22 S. M. Howdle, J. M. Ramsay and A. I. Cooper, *J. Polym. Sci. Part B: Polym. Phys.*, 1994, **32**, 541.
23 R. Zhu, Y. Wei, C. W. Yuan, S. J. Xiao, Z. H. Lu and H. J. Schmitt, *Solid State Commun.*, 1992, **84**, 449.
24 R. Tassoni and R. R. Schrock, *Chem. Mater.*, 1992, **4**, 312.
25 V. Sankaran, J. Yue and R. E. Cohen, *Chem. Mater.*, 1993, **5**, 1153.
26 Y. N. C. Chan, R. R. Schrock and R. E. Cohen, *J. Am. Chem. Soc.*, 1992, **114**, 7295.
27 F. Grohn, G. Kim, A. J. Bauer and E. J. Amis, *Macromolecules*, 2001, **34**, 2179.
28 L. K. Yeung, C. T. J. Lee, K. P. Johnston and R. M. Crooks, *Chem. Commun.*, 2001, 2290.
29 Y. P. Sun, P. Atorngitjawat and M. J. Meziani, *Langmuir*, 2001, **17**, 5707.
30 Y. P. Sun, R. Guduru, F. Lin and T. Whiteside, *Ind. Eng. Chem. Res.*, 2000, **39**, 4663.
31 Y. P. Sun, H. W. Rollins and R. Guduru, *Chem. Mater.*, 1999, **11**, 7.
32 M. Turk, P. Hils, B. Helfgen, K. Schaber, H. J. Martin and M. A. Wahl, *J. Supercrit. Fluids*, 2002, **22**, 75.
33 P. Chattopadhyay and R. B. Gupta, *Ind. Eng. Chem. Res.*, 2001, **40**, 3530.
34 M. A. McHugh and V. J. Krukonis, *Supercritical Fluid Extraction*, Butterworth-Heineman, Boston, 1994.
35 J. A. Darr and M. Poliakoff, *Chem. Rev.*, 1999, **99**, 495.
36 A. I. Cooper, *J. Mater. Chem.*, 2000, **10**, 207.
37 S. G. Kazarian, *Polym. Sci., Ser. C*, 2000, **42**, 78.
38 W. H. Hauthal, *Chemosphere*, 2001, **43**, 123.
39 S. G. Kazarian, *Appl. Spectrosc. Rev.*, 1997, **32**, 301.
40 M. Jobling, S. M. Howdle and M. Poliakoff, *J. Chem. Soc., Chem. Commun.*, 1990, 1762.
41 S. G. Kazarian, N. H. Brantley and C. A. Eckert, *Chemtech*, 1999, **29**, 36.
42 V. K. Popov, V. N. Bagratashvili, A. P. Krasnov, E. E. Said-Galiyev, L. N. Nikitin, O. V. Afonicheva and A. D. Aliev, *Tribology Lett.*, 1998, **5**, 297.
43 E. N. Antonov, V. N. Bagratashvili, O. A. Louchev, G. V. Mishakov, V. K. Popov and S. M. Howdle, *Proceedings of the 3rd International Symposium on Supercritical Fluids*, Strasbourg, 1994, vol. 3, p. 369.
44 J. J. Watkins, J. M. Blackburn and T. J. McCarthy, *Chem. Mater.*, 1999, **11**, 213.
45 J. M. Blackburn, D. P. Long and J. J. Watkins, *Chem. Mater.*, 2000, **12**, 2625.
46 D. P. Long, J. M. Blackburn and J. J. Watkins, *Adv. Mater.*, 2000, **12**, 913.
47 J. M. Blackburn, D. P. Long, A. Cabanas and J. J. Watkins, *Science*, 2001, **294**, 141.
48 E. N. Sobol, V. N. Bagratashvili, A. E. Sobol and S. M. Howdle, *Dokl. Akad. Nauk*, 1997, **356**, 777.
49 S. G. Kazarian, M. F. Vincent, F. V. Bright, C. L. Liotta and C. A. Eckert, *J. Am. Chem. Soc.*, 1996, **118**, 1729.
50 S. G. Kazarian, M. F. Vincent and C. A. Eckert, *Rev. Sci. Instrum.*, 1996, **67**, 1586.
51 J. J. Watkins and T. J. McCarthy, *Chem. Mater.*, 1995, **7**, 1991.
52 W. Leitner, *Chemical synthesis using supercritical fluids*, ed. P. G. Jessop and W. Leitner, Wiley-VCH, Weinheim, 1999.
53 C. M. Wai and B. Waller, *Ind. Eng. Chem. Res.*, 2000, **39**, 4837.
54 C. M. Wai and S. F. Wang, *J. Chromat., A*, 1997, **785**, 369.
55 M. Z. Ozel, M. D. Burford, A. A. Clifford, K. D. Bartle, A. Shadrin, N. G. Smart and N. D. Tinker, *Anal. Chim. Acta*, 1997, **346**, 73.
56 J. A. Darr, M. Poliakoff, A. J. Blake and W. S. Li, *Inorg. Chem.*, 1998, **37**, 5491.
57 J. A. Darr, M. A. Poliakoff, W. S. Li and A. J. Blake, *J. Chem. Soc., Dalton Trans.*, 1997, 2869.
58 C. J. Brinker, *Sol-gel Science: The Physics and Chemistry of Sol-gel Processing*', Academic Press, Boston, 1990.
59 S. M. Howdle, K. Jerabek, V. Leocorbo, P. C. Marr and D. C. Sherrington, *Polymer*, 2000, **41**, 7273.
60 P. B. Webb, *Modification and Processing of Polymers using Supercritical Fluids*, PhD Thesis, University of Nottingham, Nottingham, 2000.
61 M. P. Klug and L. E. Alexander, *X-ray Diffraction Procedures for Polycrystalline and Amorphous Materials*, John Wiley and Sons Inc, New York, 1970.
62 R. H. Doremus, *Glass Science*, Wiley-Interscience, New York, 1994.
63 A. J. Blake, N. R. Champness, S. M. Howdle, K. S. Morley, P. B. Webb and C. Wilson, *CrystEngComm*, 2002, **16**.
64 A. J. Blake, N. R. Champness, S. M. Howdle and P. B. Webb, *Inorg. Chem.*, 2000, **39**, 1035.
65 Y. H. Lin, H. Wu, N. Smart and C. M. Wai, *J. Chromat. A*, 1998, **793**, 107.
66 T. Kodas and M. J. Hampden-Smith, *The Chemistry of Metal CVD*, VCH: Weinheim, 1994.